nature medicine

Detecting tumor response to treatment using hyperpolarized ^{13}C magnetic resonance imaging and spectroscopy

Sam E Day[1,5], Mikko I Kettunen[1,5], Ferdia A Gallagher[1,2], De-En Hu[1], Mathilde Lerche[3], Jan Wolber[4], Klaes Golman[3], Jan Henrik Ardenkjaer-Larsen[4] & Kevin M Brindle[1]

Measurements of early tumor responses to therapy have been shown, in some cases, to predict treatment outcome. We show in lymphoma-bearing mice injected intravenously with hyperpolarized [1-^{13}C]pyruvate that the lactate dehydrogenase–catalyzed flux of ^{13}C label between the carboxyl groups of pyruvate and lactate in the tumor can be measured using ^{13}C magnetic resonance spectroscopy and spectroscopic imaging, and that this flux is inhibited within 24 h of chemotherapy. The reduction in the measured flux after drug treatment and the induction of tumor cell death can be explained by loss of the coenzyme NAD(H) and decreases in concentrations of lactate and enzyme in the tumors. The technique could provide a new way to assess tumor responses to treatment in the clinic.

Tumor responses to treatment are assessed largely from imaging measurements of tumor size. Reductions in tumor volume may take weeks, however, and therefore there has been considerable interest in the development of imaging techniques that could give early indications of response to treatment and that could predict treatment outcome[1–3]. The most widely used technique in the clinic has been positron emission tomography (PET) measurements of ^{18}F-fluorodeoxyglucose (FDG) uptake (FDG-PET). For example, in patients with gastrointestinal stromal tumors, FDG-PET–measured uptake is reduced as early as 24 h after treatment with imatinib, whereas weeks to months are required before the tumors shrink[4]. This technique has relatively poor spatial resolution, however, compared to magnetic resonance imaging (MRI), and it involves exposure of the patient to ionizing radiation.

Magnetic resonance methods for detecting early tumor responses to treatment (reviewed in ref. 5) have included measurements of the apparent diffusion coefficient of water[6]. These have been used clinically[7] and they appear to detect the reduction in tumor cellularity resulting from a positive response to treatment.

^{13}C magnetic resonance spectroscopy (MRS) has long been used in the investigation of metabolic processes *in vivo*[8]. The recent introduction of dynamic nuclear polarization (DNP) for solution-state magnetic resonance, which can increase sensitivity in the ^{13}C MRS experiment by 10,000-fold or more, now allows not only detection of ^{13}C-labeled substrates *in vivo* but imaging of their tissue distribution as well[9–13]. An additional advantage is that there is no background signal from nonpolarized material. We show here that flux of hyperpolarized ^{13}C label between pyruvate and lactate in the reaction catalyzed by lactate dehydrogenase (LDH) is decreased in mouse lymphoma cells *in vitro* and in lymphoma tumors *in vivo* after drug-induced cell death.

RESULTS

Measurements in cells

After addition of hyperpolarized [1-^{13}C]pyruvate to EL-4 mouse lymphoma cells, the lactate carboxyl signal (**Fig. 1a**) first increased, as label was transferred from pyruvate, and then decreased owing to decay of the polarization, which has an apparent spin lattice relaxation time, T_1, of ~40 s (**Fig. 1b**). The unassigned signals (**Fig. 1a**) are from minor contaminants in the pyruvate preparation. There was no evidence that these contaminants were metabolized by the cells, and their signals were not observed *in vivo*.

The peak intensities for labeled pyruvate and lactate can be fit to the modified Bloch equations for two-site exchange (equations (2) and (3))[14].

$$\mathrm{L} \underset{k_{\mathrm{P}}}{\overset{k_{\mathrm{L}}}{\rightleftharpoons}} P \tag{1}$$

$$\mathrm{d}L_z/\mathrm{d}t = -\rho_{\mathrm{L}}(L_z - L_\infty) + k_{\mathrm{P}}P_z - k_{\mathrm{L}}L_z \tag{2}$$

$$\mathrm{d}P_z/\mathrm{d}t = -\rho_{\mathrm{P}}(P_z - P_\infty) + k_{\mathrm{L}}L_z - k_{\mathrm{P}}P_z \tag{3}$$

L and P denote lactate and pyruvate, respectively; t is time; L_z and P_z are the z-magnetizations of the ^{13}C nucleus in the lactate and pyruvate

[1]Cancer Research UK, Cambridge Research Institute, Li Ka Shing Centre, Robinson Way, Cambridge CB2 0RE, UK, and Department of Biochemistry, University of Cambridge, Tennis Court Road, Cambridge CB2 1GA, UK. [2]Department of Radiology, University of Cambridge, Level 5, Box 219 Addenbrooke's Hospital, Hills Road, Cambridge CB2 2QQ, UK. [3]Imagnia AB, Box 8225 200 41, Malmö, Sweden. [4]GE Healthcare, The Grove Centre GC/18, White Lion Road, Amersham HP7 9LL, UK. [5]These authors contributed equally to this work. Correspondence should be addressed to K.M.B. (kmb@mole.bio.cam.ac.uk).

Received 24 April; accepted 14 August; published online 28 October 2007; corrected after print 12 November 2007; doi:10.1038/nm1650

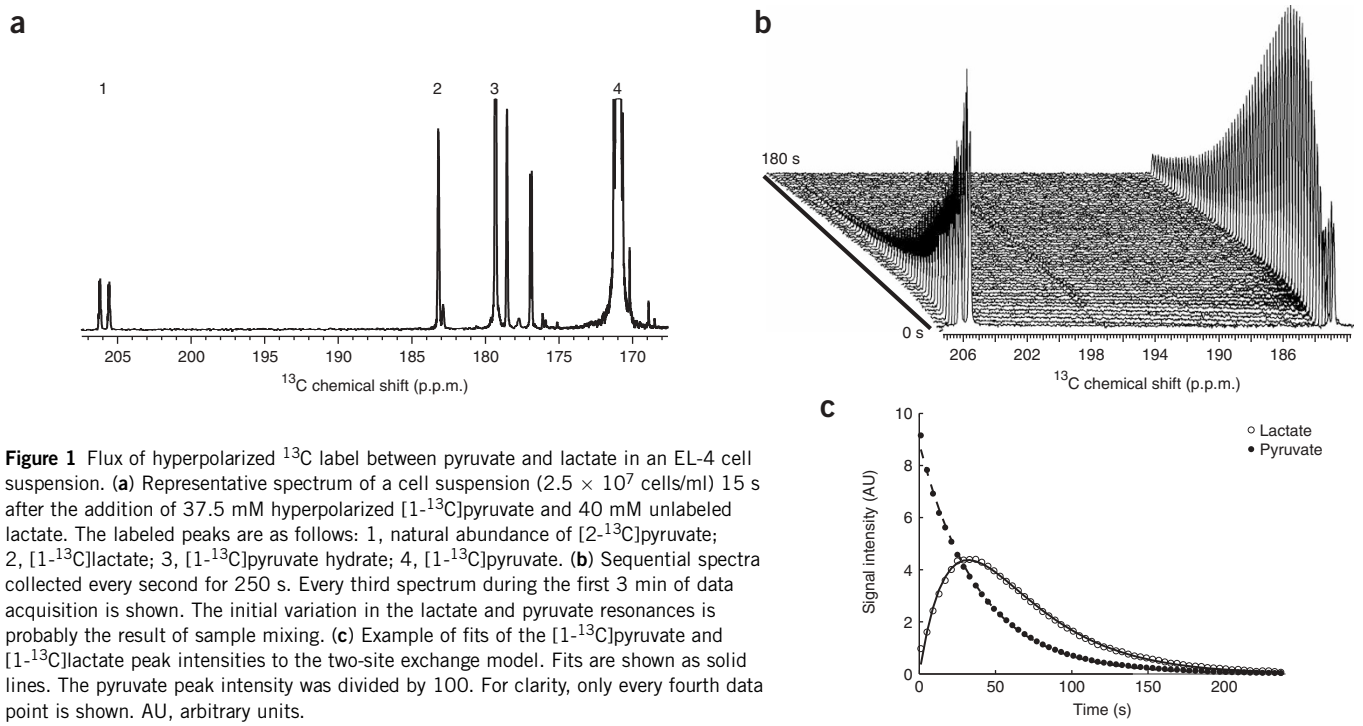

Figure 1 Flux of hyperpolarized ^{13}C label between pyruvate and lactate in an EL-4 cell suspension. (**a**) Representative spectrum of a cell suspension (2.5×10^7 cells/ml) 15 s after the addition of 37.5 mM hyperpolarized [1-^{13}C]pyruvate and 40 mM unlabeled lactate. The labeled peaks are as follows: 1, natural abundance of [2-^{13}C]pyruvate; 2, [1-^{13}C]lactate; 3, [1-^{13}C]pyruvate hydrate; 4, [1-^{13}C]pyruvate. (**b**) Sequential spectra collected every second for 250 s. Every third spectrum during the first 3 min of data acquisition is shown. The initial variation in the lactate and pyruvate resonances is probably the result of sample mixing. (**c**) Example of fits of the [1-^{13}C]pyruvate and [1-^{13}C]lactate peak intensities to the two-site exchange model. Fits are shown as solid lines. The pyruvate peak intensity was divided by 100. For clarity, only every fourth data point is shown. AU, arbitrary units.

carboxyl carbons; ρ_L and ρ_P are the spin lattice relaxation rates ($1/T_{1(L,P)}$); and L_∞ and P_∞ are the equilibrium magnetizations (that is, at $t = \infty$) of lactate and pyruvate, which are effectively equivalent to their concentrations. The lactate and pyruvate peak intensities were fit to these equations (see Methods) to obtain the rate constants k_L and k_P and the apparent spin lattice relaxation rates (**Fig. 1c**). L_∞/P_∞ was obtained from the ratio of the fitted rate constants. Because we used low–flip angle pulses, we ignored the effects of repeated excitation on decay of the polarization (**Supplementary Figs. 1** and **2** online). The rate constants reflect LDH activity, membrane transport of lactate and pyruvate and, *in vivo*, pyruvate delivery to the tumor. We may also have detected signals from several compartments in the tissue. Therefore, the estimated rate constants are apparent rate constants (k_{app}). Addition of unlabeled lactate to the cells increased the rate constants and the amplitude of the lactate ^{13}C peak intensity (**Fig. 2a**), consistent with exchange of ^{13}C label between lactate and pyruvate at or near chemical equilibrium[15] (**Supplementary Fig. 3** online).

Treatment with 15 μM etoposide for 16 h resulted in 30%–40% apoptosis, 10%–15% necrosis and an approximately 80% reduction in flux ($k_{app(P)} \times [P]$), from 54 ± 15 nmol/s/10^8 cells ($n = 4$) to 9.0 ± 1.5 nmol/s/10^8 cells ($n = 5$, $P < 0.005$; **Fig. 2b**). There was negligible loss of LDH activity in cell extracts: LDH activity was 5.43 ± 0.34 units/10^7 cells ($n = 3$) in control cells and 5.37 ± 0.27 units/10^7 cells ($n = 3$) in drug-treated cells. The cell counts included viable, apoptotic and necrotic cells. After 20 h of incubation with etoposide, however, when the necrotic fraction increased from ~15% to ~45%, the LDH activity decreased significantly to 2.53 ± 0.32 units/10^7 cells ($n = 3$, $P < 0.01$).

We confirmed the levels of necrosis and apoptosis by flow cytometry, measuring 40%–50% apoptotic cells and 20% necrotic cells[16]. The apoptotic cell population was evident as a population with low UV autofluorescence (**Fig. 3a**). This has been observed previously[17] and is probably the result of poly(ADP-ribose) polymerase (PARP)-mediated depletion of the NAD(H) pool[18]. ^{31}P MRS measurements of extracts (**Fig. 3b**) showed that the NAD$^+$ concentration decreased

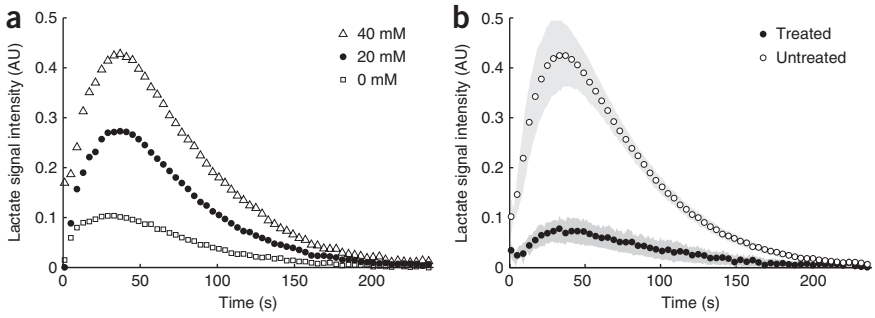

Figure 2 Effect of addition of exogenous lactate and induction of cell death on flux of hyperpolarized ^{13}C label between pyruvate and lactate in an EL-4 cell suspension. (**a**) [1-^{13}C]lactate peak intensities after addition of 37.5 mM hyperpolarized [1-^{13}C]pyruvate and the specified lactate concentration to an EL-4 cell suspension (2.5×10^7 cells/ml). Spectra were scaled to the initial pyruvate signal intensity to correct for variation in polarization levels. For clarity, only every fourth data point is shown. (**b**) [1-^{13}C]lactate peak intensities after addition of 37.5 mM hyperpolarized [1-^{13}C]pyruvate and 40 mM unlabeled lactate to EL-4 cell suspensions (2.5×10^7 cells/ml) that had been treated for 16 h with 15 μM etoposide or were untreated. For clarity, only every fourth data point is shown. Shaded regions represent one s.d. from the mean value ($n = 3$ for both groups). The total number of cells (viable, apoptotic and necrotic) was the same in both experiments. AU, arbitrary units.

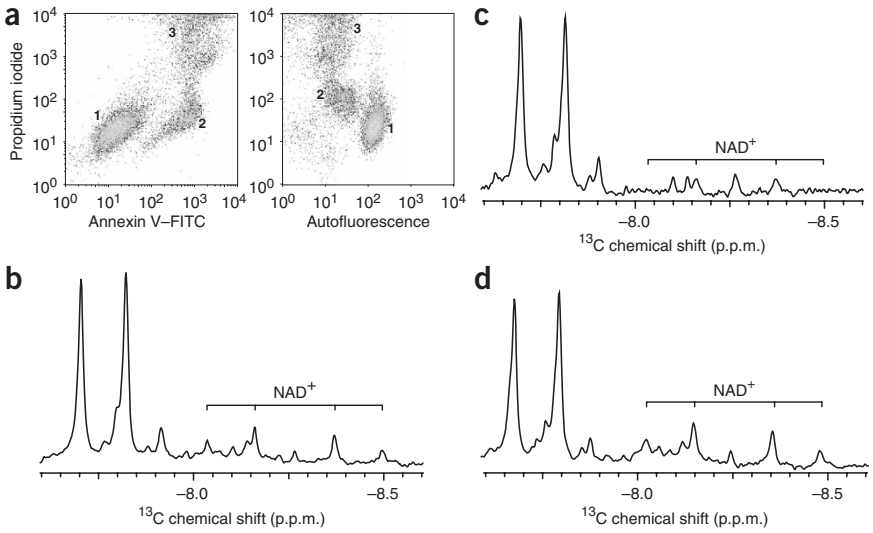

Figure 3 Induction of cell death depletes EL-4 cells of NAD(H). (**a**) Flow-cytometric analysis of cells treated for 16 h with 15 μM etoposide. Apoptotic cells were detected using annexin V–FITC ($\lambda_{excitation}$ = 488 nm, $\lambda_{emission}$ = 518 nm) and necrotic cells using propidium iodide ($\lambda_{excitation}$ = 535 nm, $\lambda_{emission}$ = 617 nm). The autofluorescence observed at 442 nm after excitation at 346 nm has been assigned to NADH. Population 1 represents viable cells, whereas population 2 represents apoptotic cells, which show little UV autofluorescence, indicating depletion of NADH. Population 3 represents necrotic cells. (**b**–**d**) ^{31}P NMR spectra of perchloric acid extracts of EL-4 cells that were either untreated (**b**), treated for 16 h with 15 μM etoposide (**c**) or treated for 16 h with 15 μM etoposide and 20 mM nicotinamide (**d**). Resonances from NAD$^+$ are indicated. Resonances from fructose-1,6-bisphosphate, which are not shown, were at 7.0 and 7.15 p.p.m.

from 0.53 ± 0.26 to 0.27 ± 0.14 nmol/10^6 cells (n = 3) and that the fructose-1,6-bisphosphate concentration increased from 0.22 ± 0.06 to 0.56 ± 0.07 nmol/10^6 cells (n = 3) in etoposide-treated cells. Accumulation of fructose-1,6-bisphosphate is caused by inhibition of the glycolytic enzyme glyceraldehyde-3-phosphate dehydrogenase, resulting from loss of the NAD(H) pool[19]. Administration of a PARP inhibitor, nicotinamide, inhibited loss of NAD$^+$ (0.77 ± 0.18 nmol/10^6 cells, n = 3; **Fig. 3c,d**) and the accumulation of fructose-1,6-bisphosphate (0.13 ± 0.06 nmol/10^6 cells, n = 3). Addition of nicotinamide also largely prevented the loss of lactate-pyruvate exchange, suggesting that the decreased flux in dying cells resulted mainly from the loss of NAD(H) and the consequent decrease in LDH activity. The flux was 42 ± 11 nmol/s/10^8 cells (n = 4) in cells incubated with etoposide and 20 mM nicotinamide. Addition of another PARP inhibitor, 3-aminobenzamide[20], also inhibited loss of lactate-pyruvate exchange, which was 27 ± 2 nmol/s/10^8 cells (n = 2) in cells treated with the drug plus 10 mM 3-aminobenzamide.

Measurements in tumors

We produced lymphoma tumors in mice by subcutaneous implantation of EL-4 cells. Intravenous injection of hyperpolarized [1-^{13}C]pyruvate (0.2 ml, 75 mM) resulted in signals from [1-^{13}C]pyruvate and lactate in the tumor (**Fig. 4a**). Measurements from an imaging slice in underlying muscle and from a slice that passed through the liver above the tumor showed substantial signal from pyruvate but only small signals from lactate in drug-treated and untreated mice

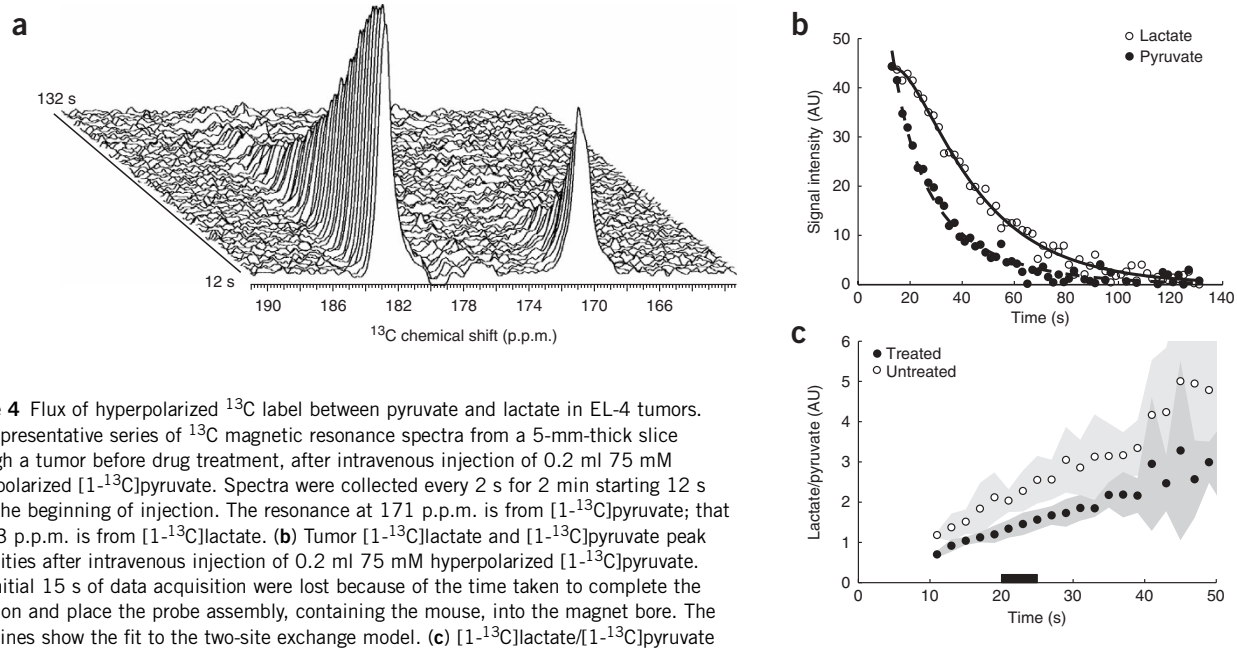

Figure 4 Flux of hyperpolarized ^{13}C label between pyruvate and lactate in EL-4 tumors. (**a**) Representative series of ^{13}C magnetic resonance spectra from a 5-mm-thick slice through a tumor before drug treatment, after intravenous injection of 0.2 ml 75 mM hyperpolarized [1-^{13}C]pyruvate. Spectra were collected every 2 s for 2 min starting 12 s after the beginning of injection. The resonance at 171 p.p.m. is from [1-^{13}C]pyruvate; that at 183 p.p.m. is from [1-^{13}C]lactate. (**b**) Tumor [1-^{13}C]lactate and [1-^{13}C]pyruvate peak intensities after intravenous injection of 0.2 ml 75 mM hyperpolarized [1-^{13}C]pyruvate. The initial 15 s of data acquisition were lost because of the time taken to complete the injection and place the probe assembly, containing the mouse, into the magnet bore. The solid lines show the fit to the two-site exchange model. (**c**) [1-^{13}C]lactate/[1-^{13}C]pyruvate peak intensity ratios in untreated and drug-treated tumors. Data were collected 20 h after injection of the mice with etoposide. Shaded regions represent one s.d. from the mean (n = 8 for both groups). Black bar between 20 and 25 s indicates the time period when spectroscopic imaging was performed (see **Fig. 5**). AU, arbitrary units.

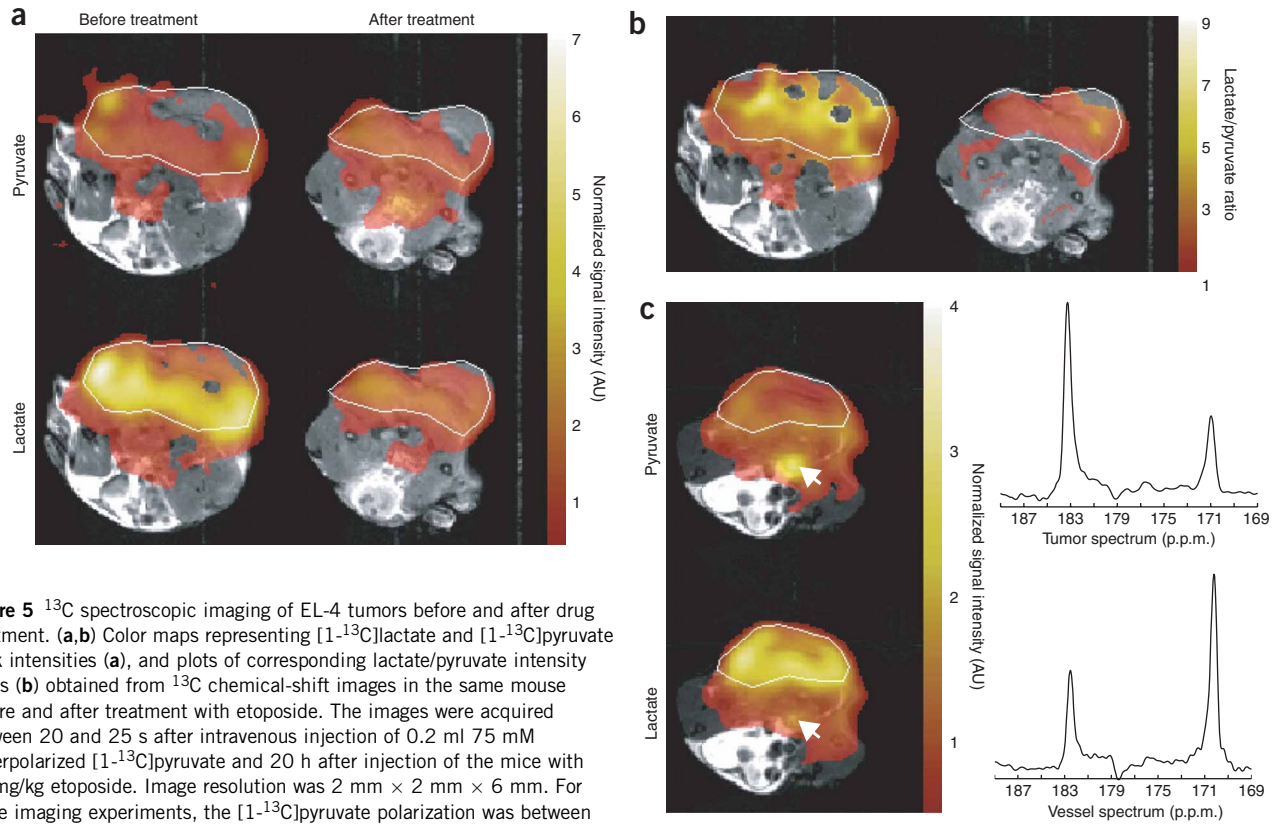

Figure 5 ^{13}C spectroscopic imaging of EL-4 tumors before and after drug treatment. (**a**,**b**) Color maps representing [1-^{13}C]lactate and [1-^{13}C]pyruvate peak intensities (**a**), and plots of corresponding lactate/pyruvate intensity ratios (**b**) obtained from ^{13}C chemical-shift images in the same mouse before and after treatment with etoposide. The images were acquired between 20 and 25 s after intravenous injection of 0.2 ml 75 mM hyperpolarized [1-^{13}C]pyruvate and 20 h after injection of the mice with 67 mg/kg etoposide. Image resolution was 2 mm × 2 mm × 6 mm. For these imaging experiments, the [1-^{13}C]pyruvate polarization was between 23% and 30%. To account for differences in polarization, the pre- and post-treatment data were normalized so that the mean pyruvate signal in the tumor was 1. AU, arbitrary units. (**c**) Color maps representing [1-^{13}C]lactate and [1-^{13}C]pyruvate peak intensities and spectra from the tumor and a blood vessel (indicated by arrow) in an etoposide-treated mouse. The ^{1}H images, shown in grayscale, were used to define the tumor margins (indicated by white lines).

(**Supplementary Fig. 4** online). We fitted the changes in the tumor lactate and pyruvate signals to the exchange model to obtain the apparent rate constants and spin lattice relaxation times (**Fig. 4b**).

Treatment of mice with etoposide resulted in the death of 37% ± 4% of tumor cells 24 h after drug treatment, as compared to 5% ± 1% in the control group ($n = 3$, $P < 0.01$), and there was a small decrease in tumor volume, from 1.6 ± 0.4 cm^3 ($n = 8$) to 1.3 ± 0.2 cm^3 ($n = 8$). Drug treatment resulted in an ~25% decrease in the rate constant $k_{\mathrm{app(P)}}$, from 0.075 ± 0.011 s^{-1} to 0.056 ± 0.005 s^{-1} ($n = 8$, $P < 0.01$). Pyruvate concentrations, determined by ^{1}H NMR measurements of extracts of freeze-clamped tumors, were 0.55 ± 0.19 μmol per gram of wet weight ($n = 8$) in control tumors and 0.75 ± 0.48 μmol per gram of wet weight ($n = 8$) in drug-treated tumors. The decreased flux between pyruvate and lactate could be seen in a plot of the labeled lactate/pyruvate ratios (**Fig. 4c**). The calculated equilibrium lactate/pyruvate ratios (that is, L_∞/P_∞, equivalent to the concentration ratios) decreased from 4.0 ± 0.8 ($n = 8$) in control tumors to 2.7 ± 0.4 ($n = 8$, $P < 0.005$) in etoposide-treated tumors. A similar decrease was observed for the lactate/pyruvate ratio measured by ^{1}H NMR in extracts of freeze-clamped tumors, in which the ratio decreased from 9.5 ± 3.5 ($n = 8$) to 5.1 ± 2.0 ($n = 8$, $P < 0.01$). We made these extracts immediately after completion of the magnetic resonance experiments. The lactate concentrations in treated and untreated tumors from mice that had not been injected with pyruvate were 3.6 ± 0.2 μmol per gram of wet weight and 3.0 ± 0.6 μmol per gram of wet weight ($n = 3$), respectively, and were not statistically significantly different from those in pyruvate-injected mice, which were 3.2 ± 1.3 μmol per gram of wet weight and 5.0 ± 1.9 μmol per gram of wet weight, respectively ($n = 8$ for each group). The LDH activity measured in tumor extracts decreased from 350 ± 200 units per gram of wet weight ($n = 5$) to 100 ± 20 units per gram of wet weight ($n = 3$, $P < 0.05$) in drug-treated tumors.

In another experiment, we treated mice with the drug 24 h after imaging, and then 24 h later we acquired additional images; thus, each mouse served as its own control. The rate constant was 0.065 ± 0.017 s^{-1} before treatment and 0.040 ± 0.012 s^{-1} after treatment ($n = 4$, $P < 0.01$), a 39% decrease.

^{13}C chemical-shift images from a tumor before and after treatment are shown in **Figure 5**. These images reveal heterogeneity in the lactate/pyruvate ratio (see also **Supplementary Fig. 5** online) and a marked reduction of this ratio in the treated tumor. In some images we could see blood vessels (**Fig. 5c**), which contained labeled pyruvate but only relatively low concentrations of labeled lactate.

DISCUSSION

Measurements of hyperpolarized ^{13}C label flux between pyruvate and lactate can be used to detect responses to chemotherapy in isolated tumor cells and in tumors *in vivo*, where the induction of cell death results in decreased flux. Exchange of label makes a substantial contribution to the measured flux from pyruvate to lactate. This was shown in the experiments with isolated cells, in which the addition of exogenous lactate increased flux, and also in the experiments with tumors, in which the equilibrium concentration ratio of

lactate and pyruvate (L_∞/P_∞), calculated from the fitted rate constants $k_{app(P)}$ and $k_{app(L)}$, was comparable to the lactate and pyruvate concentrations measured in tumor extracts. *In vivo*, however, there may also be net flux from pyruvate to lactate. The relatively low concentrations of labeled lactate in the blood and in other tissues suggest that there is little influx into the tumor of labeled lactate from the circulation.

Fitting both the pyruvate and lactate peak intensities to the kinetic model corrected, to some extent, for any differences in pyruvate delivery to the tumor and for the B_1 inhomogeneity of the detector coil. The inhibition of flux in responding tumors could also be detected as a decrease in the labeled lactate/pyruvate ratio in ^{13}C chemical shift images. The imaging experiments could be improved by increasing the speed of image acquisition, which would allow the acquisition of a series of images and thus the calculation of an enzyme activity map.

Induction of apoptosis by a chemotherapeutic drug, etoposide, resulted in a significant reduction in flux ($P = 0.0002$ *in vitro* and $P = 0.0010$ *in vivo*). In the cells, this reduction resulted mainly from a loss of the coenzyme NAD(H). Loss of exchange after extended incubation with the drug, when the frequency of necrosis increased, can also be explained by loss of LDH from the cells. The decrease in flux in treated tumors was probably the result of NAD(H) loss and the measured decreases in extractable tumor LDH activity and lactate concentration. A decrease in lactate concentration has been observed previously in treated tumors using localized ^{1}H MRS measurements[21,22].

A limitation of the tumor model we used is its rapid response to treatment; there was a 17% decrease in tumor volume by 24 h. It will be of interest to determine whether this and other techniques can be used to detect responses sooner after treatment.

Because pyruvate is an endogenous substrate, we expect that this technique could transfer to the clinic, and it has an advantage over other MRS techniques[21–23] in that it allows rapid spectroscopic imaging of the response. The advantages of this technique over FDG-PET will need to be evaluated in preclinical and clinical studies. When the overall frequency of tumor cell death is low, detection using either technique may be difficult. If cell death is localized in specific regions, however, as was the case here, then the higher resolution of hyperpolarized ^{13}C MRI may be an advantage.

METHODS

Cell culture. We cultured EL-4 cells and detected apoptosis and necrosis by staining with acridine orange and propidium iodide and by flow cytometry as described previously[16,24] (see **Supplementary Methods** online).

Tumor implantation. We established tumors as described previously[16,25] and allowed them to grow for 10 d (volume, ~2 cm^3; maximum diameter, 1.5 cm). We treated mice with an intraperitoneal injection of 67 mg etoposide (PCH Pharmachemie BV) per kg body weight. We carried out our procedures under the authority of project and personal licenses issued by the Home Office, United Kingdom. We assessed tumor cell death histologically[16].

[1-^{13}C]pyruvate hyperpolarization. We hyperpolarized a 44-mg sample of 91% [1-^{13}C]pyruvic acid containing 15 mM of the trityl radical OXO63 (GE Healthcare) as described previously[9]. We dissolved the frozen sample at 180 °C in 6 ml buffer containing 40 mM HEPES, 94 mM NaOH, 30 mM NaCl and 50 mg/l EDTA. The sample was dissolved and removed from the polarizer magnet in less than 10 s, and the same preparation was used for the cell and tumor experiments. The polarization levels were 12%–15%, unless stated otherwise.

Nuclear magnetic resonance spectroscopy of cells. We examined cells (10^8) in RPMI 1640 medium in a 10-mm NMR tube, using a broadband probe (Varian) in a 9.4-T vertical wide-bore magnet (Oxford Instruments). We maintained the temperature at 37 °C. We injected hyperpolarized [1-^{13}C]pyruvate (75 mM) and non-hyperpolarized, unlabeled lactate (40 or 80 mM) and acquired single transient ^{13}C spectra every second for 250 s using a 6° flip angle pulse and a spectral width of 32 kHz.

Nuclear magnetic resonance spectroscopy of tumors. We anesthetized mice by intraperitoneal administration of 10 ml per kg body weight of a 5:4:31 mixture of Hypnorm (VetaPharma), Hypnovel (Roche) and saline. We inserted a catheter into a tail vein and positioned a 1-cm-diameter surface coil tuned to ^{13}C (100 MHz) over the tumor. We placed the entire assembly in a quadrature ^{1}H-tuned volume coil (Varian), in a 9.4-T vertical wide-bore magnet. We acquired transverse ^{1}H images using a spin-echo pulse sequence (repetition time (TR), 1.5 s; echo time (TE), 30 ms; field of view, 32 mm × 32 mm; data matrix, 256 × 256; slice thickness, 2 mm; 11 slices). After injection of hyperpolarized [1-^{13}C]pyruvate, accomplished within 3 s, we collected 160 interleaved single transient spectra over a period of 160 s from the entire sensitive volume of the surface coil and from a 5-mm-thick tumor slice (80 spectra from each volume). We used a pulse-acquire sequence with a slice-selective 600-μs sinc pulse, with a nominal flip angle of 5°, for slice selection.

Imaging. We acquired transverse ^{13}C chemical-shift images from a 6-mm slice through the tumor mass between 20 and 25 s after injection of hyperpolarized [1-^{13}C]pyruvate. The imaging sequence was the same as that used for the spectroscopic measurements, with additional phase-encoding gradients preceding signal acquisition (TR, 20 ms; TE, 1.5 ms; field of view, 32 mm × 32 mm; data matrix, 16 × 16; spectral width, 8 kHz; total acquisition time, 5 s).

Data analysis. The peak integrals from [1-^{13}C]pyruvate and [1-^{13}C]lactate were fit to the following equations with Matlab Mathworks:

$$L_z - L_\infty = \frac{k_P P_\infty (Z-1)}{(\lambda^+ - \lambda^-)}(e^{\lambda^+ t} - e^{\lambda^- t}) \quad (4)$$

$$P_z - P_\infty = \frac{P_\infty (Z-1)}{(\lambda^+ - \lambda^-)}((\rho_L + k_L + \lambda^+)e^{\lambda^+ t} - (\rho_L + k_L + \lambda^-)e^{\lambda^- t}) \quad (5)$$

$$\lambda^\pm = \frac{-(\rho_L + k_L + \rho_P + k_P) \pm \sqrt{((\rho_L + k_L) - (\rho_P + k_P))^2 + 4k_L k_P}}{2} \quad (6)$$

λ denotes the roots of the quadratic equation. At $t = 0$, $P_z = ZP_\infty$ and $L_z = L_\infty$, where Z is the degree of polarization. We assumed that L_∞ and P_∞ are given by the concentrations of lactate and pyruvate, respectively. The nonpolarized ^{13}C content was ignored, as its signal is negligible. The relaxation rates for lactate and pyruvate were assumed to be the same. We calculated maps of lactate/pyruvate ratios from ^{13}C chemical-shift images. We zero-filled the data to 128 × 128 and calculated the peak integrals from baseline-corrected data in absolute-value mode. We set the lactate/pyruvate ratios to 0 in pixels where either the lactate or pyruvate intensities were less than 10% of the corresponding maximum intensities.

Tumor extracts. We snap-froze rapidly excised tumors in a liquid nitrogen–cooled mortar, extracted samples using 7% ice-cold perchloric acid and acquired ^{1}H NMR spectra from the neutralized samples (**Supplementary Methods**).

For measurements of LDH activity, we thawed tumor tissue in 50 mM Tris-HCl (pH 8.2), 2 mM dithiothreitol, 2 mM EDTA and 1% Triton X-100, and then homogenized it using a tight-fitting Potter homogenizer. We assayed extracts as described in ref. 26 and **Supplementary Methods**.

Cell extracts. We extracted cells (6 × 10^8) using 7% ice-cold perchloric acid and acquired ^{31}P spectra from the neutralized samples (**Supplementary Methods**). For measurements of LDH activity, we resuspended 10^7 cells in 50 mM Tris-HCl (pH 8.2), 2 mM dithiothreitol, 2 mM EDTA and 1% Triton X-100, and then homogenized the mixture using a tight-fitting Potter homogenizer. We assayed extracts as described in ref. 26 and **Supplementary Methods**.

Additional methods. Detailed methodology is described in **Supplementary Methods**.

Note: Supplementary information is available on the Nature Medicine website.

ACKNOWLEDGMENTS
F.A.G. received a Cancer Research UK and Royal College of Radiologists (UK) clinical research training fellowship, and S.E.D. received a US National Institutes of Health–Cambridge studentship. This work was supported by a Cancer Research UK programme grant to K.M.B. (C197/A3514). The polarizer and related materials were provided by GE Healthcare.

AUTHOR CONTRIBUTIONS
S.E.D. conducted the cell experiments and operated the polarizer with F.A.G. M.I.K. was responsible for MRS and imaging experiments. S.E.D., F.A.G. and M.I.K. were jointly responsible for data analysis. D.-E.H. was responsible for tumor implantation and animal handling during the MRS experiments. M.L., J.W., K.G. and J.H.A.-L. provided advice and assistance with the pyruvate preparation and operation of the polarizer. K.M.B. organized the study, devised the kinetics analysis and wrote the paper.

COMPETING INTERESTS STATEMENT
The authors declare competing financial interests: details accompany the full-text HTML version of the paper at http://www.nature.com/naturemedicine.

Published online at http://www.nature.com/naturemedicine
Reprints and permissions information is available online at http://npg.nature.com/reprintsandpermissions

1. Neves, A.A. & Brindle, K.M. Assessing responses to cancer therapy using molecular imaging. *Biochim. Biophys. Acta* **1766**, 242–261 (2006).
2. Czernin, J., Weber, W.A. & Herschman, H.R. Molecular imaging in the development of cancer therapeutics. *Annu. Rev. Med.* **57**, 99–118 (2006).
3. Weber, W.A. Positron emission tomography as an imaging biomarker. *J. Clin. Oncol.* **24**, 3282–3292 (2006).
4. Stroobants, S. *et al.* (18)FDG-Positron emission tomography for the early prediction of response in advanced soft tissue sarcoma treated with imatinib mesylate (Glivec). *Eur. J. Cancer* **39**, 2012–2020 (2003).
5. Kettunen, M.I. & Brindle, K.M. Apoptosis detection using magnetic resonance imaging and spectroscopy. *Prog. Nucl. Magn. Reson. Spectrosc.* **47**, 175–185 (2005).
6. Ross, B.D. *et al.* Evaluation of cancer therapy using diffusion magnetic resonance imaging. *Mol. Cancer Ther.* **2**, 581–587 (2003).
7. Moffat, B.A. *et al.* Functional diffusion map: A noninvasive MRI biomarker for early stratification of clinical brain tumor response. *Proc. Natl. Acad. Sci. USA* **102**, 5524–5529 (2005).
8. Shulman, R.G. *et al.* Cellular applications of ^{31}P and ^{13}C nuclear magnetic resonance. *Science* **205**, 160–166 (1979).
9. Ardenkjaer-Larsen, J.H. *et al.* Increase in signal-to-noise ratio of $>$ 10,000 times in liquid-state NMR. *Proc. Natl. Acad. Sci. USA* **100**, 10158–10163 (2003).
10. Golman, K., Ardenkjær-Larsen, J.H., Petersson, J.S., Månsson, S. & Leunbach, I. Molecular imaging with endogenous substances. *Proc. Natl. Acad. Sci. USA* **100**, 10435–10439 (2003).
11. Golman, K., in 't Zandt, R. & Thaning, M. Real-time metabolic imaging. *Proc. Natl. Acad. Sci. USA* **103**, 11270–11275 (2006).
12. Golman, K. & Petersson, J.S. Metabolic imaging and other applications of hyperpolarized ^{13}C. *Acad. Radiol.* **13**, 932–942 (2006).
13. Golman, K., Zandt, R.I., Lerche, M., Pehrson, R. & Ardenkjaer-Larsen, J.H. Metabolic imaging by hyperpolarized 13C magnetic resonance imaging for *in vivo* tumor diagnosis. *Cancer Res.* **66**, 10855–10860 (2006).
14. Brindle, K.M. NMR methods for measuring enzyme kinetics *in vivo*. *Prog. Nucl. Magn. Reson. Spectrosc.* **20**, 257–293 (1988).
15. Brindle, K.M., Campbell, I.D. & Simpson, R.J. A ^{1}H-NMR study of the activity expressed by lactate dehydrogenase in the human erythrocyte. *Eur. J. Biochem.* **158**, 299–305 (1986).
16. Schmitz, J.E., Kettunen, M.I., Hu, D.E. & Brindle, K.M. ^{1}H MRS-visible lipids accumulate during apoptosis of lymphoma cells *in vitro* and *in vivo*. *Magn. Reson. Med.* **54**, 43–50 (2005).
17. Poot, M. & Pierce, R.H. Detection of changes in mitochondrial function during apoptosis by simultaneous staining with multiple fluorescent dyes and correlated multiparameter flow cytometry. *Cytometry* **35**, 311–317 (1999).
18. Sims, J.L., Berger, S.J. & Berger, N.A. Poly(ADP-ribose) polymerase inhibitors preserve nicotinamide adenine dinucleotide and adenosine 5′-triphosphate pools in DNA-damaged cells: mechanism of stimulation of unscheduled DNA synthesis. *Biochemistry* **22**, 5188–5194 (1983).
19. Williams, S.N.O., Anthony, M.L. & Brindle, K.M. Induction of apoptosis in two mammalian cell lines results in increased levels of fructose-1,6-bisphosphate and CDP-choline as determined by ^{31}P MRS. *Magn. Reson. Med.* **40**, 411–420 (1998).
20. Filipovic, D.M., Meng, X. & Reeves, W.B. Inhibition of PARP prevents oxidant-induced necrosis but not apoptosis in LLC-PK1 cells. *Am. J. Physiol.* **277**, F428–F436 (1999).
21. Aboagye, E.O., Bhujwalla, Z.M., Shungu, D.C. & Glickson, J.D. Detection of tumour response to chemotherapy by ^{1}H nuclear magnetic resonance spectroscopy: Effect of 5-fluorouracil on lactate levels in radiation-induced fibrosarcoma I tumours. *Cancer Res.* **58**, 1063–1067 (1998).
22. Poptani, H. *et al.* Detecting early response to cyclophosphamide treatment of RIF-1 tumors using selective multiple quantum spectroscopy (SelMQC) and dynamic contrast enhanced imaging. *NMR Biomed.* **16**, 102–111 (2003).
23. Hakumaki, J.M., Poptani, H., Sandmair, A-M., Yla-Herttuala, S. & Kauppinen, R.A. ^{1}H MRS detects polyunsaturated fatty acid accumulation during gene therapy of glioma: Implications for the *in vivo* detection of apoptosis. *Nat. Med.* **5**, 1323–1327 (1999).
24. Anthony, M.L., Zhao, M. & Brindle, K.M. Inhibition of phosphatidylcholine biosynthesis following induction of apoptosis in HL-60 cells. *J. Biol. Chem.* **274**, 19686–19692 (1999).
25. Zhao, M., Beauregard, D.A., Loizou, L., Davletov, B. & Brindle, K.M. Non-invasive detection of apoptosis using magnetic resonance imaging and a targeted contrast agent. *Nat. Med.* **7**, 1241–1244 (2001).
26. Vassault, A. Lactate dehydrogenase. in *Methods of Enzymatic Analysis* Vol. 3 (ed. Bergmeyer, H.U.) 118–126 (Verlag Chemie, Deerfield Beach, Florida, 1983).